Towards artificial photosynthesis : resolving supramolecular packing of artificial antennae chromophores through a hybrid approach

Thomas, B.

Chapter 4

Structural analysis of DATZnS(4H) using homology modelling

Abstract

The packing of DATZnS(4H) is deduced from CP/MAS NMR, TEM, and unit cell parameter optimization with force field modelling. C_2 molecular symmetry of the DATZnS(4H) is obtained from MAS NMR and DFT modeling. Spatial correlations obtained from HETCOR spectra collected with a long mixing time of 2 ms point towards an antiparallel stacking. The packing constraints and limited data from Fourier transformation of a TEM image are used to construct a structural model with the $P2/c$ space group obtained from the DATZnS(3′-NMe) parent compound for which the structure has been solved (chapter 2). The data indicates that the packing of fused naphthalene diimide-salphen bichromophoric antenna forming a phenazine motif with a dipole moment in a $P2/c$ supramolecular scaffold can be steered by a functional group between antiparallel dipoles and parallel dipoles in a layer. The packing of fused NDI-salphen chromophores forming a phenazine motif with a dipole moment in a $P2/c$ supramolecular scaffold can be steered by chemical substituents between antiparallel dipoles and parallel dipoles in a sheet.

4.1 Introduction

With the looming energy crisis and pollution coming out of conventional fuels, scientists are trying to find an alternative by mimicking the primary processes of photosynthesis.[1-6] In nature, plants harvest light for solar to fuel conversion using photosynthetic antennae complexes.[7-9] Even though nature has given the blue prints to convert energy from sunlight through photosynthesis, a principal challenge lies in finding suitable molecules that mimic the chemical characteristics of chlorophylls for application in artificial systems.[10-12] Self-assembly is the underlying principle behind the antenna complexes that harvest the solar flux efficiently.[13] Unique features of antenna complexes in photosynthesis is their well-

defined three dimensional architecture, which plays a significant role in absorbing the sunlight and funnel the resulting excited-state energy to a designated site.[14-16] The challenge is to find a suitable scaffold, which has the ability to harvest light into which the water splitting catalyst can be attached.[6,17]

DATZnS(4H) is a bichromophoric antenna, which is prepared by fusing naphthalene diimide with zinc salphen, thereby generating a phenazine bridge (Figure 4.1).[18-22] This molecule belongs to a class of molecules, which exhibit the properties of zinc salphen to form a metal organic framework while the NDI and the phenazine can be involved in π-π stacking.[18-20] In addition, the extended π conjugation from the salphen to NDI in the molecule enhances the π-π stacking.[21] The opto-electronic tunability[22] due to the possibility to substitute various heteroatoms and functional groups makes this molecule a versatile building block for chemical engineering purposes.[23,24] The aliphatic tails present in the molecule are an added advantage. They enhance the solubility and allow for modification at a later stage, *e.g.* by using them as a linker to attach antenna systems to functionalized electrode surfaces. The vacant orbitals present in the Zn^{2+} of the salphen can accommodate an additional ligand. For instance, a catalyst can be attached through a coordination bond to the scaffold.[14,25-27]The phenazine molecule possesses an aromatic surface which is flat and electron rich.[28] This creates the possibility of attractive van der Waals and charge transfer interactions similar to supramolecules built from porphyrins.[29-32] The properties and applications of these organometallic frameworks can be altered by changing the Zn^{2+} by other metals or by introducing a functionalized ligand. The efficiency of light harvesting and possibly also charge separation depends on the packing of the molecule in a three dimensional framework. The packing effects that derive from the scaffolding play a crucial role in determining the functional properties of these antenna complexes, such as mixing in charge transfer states into the excited state.[33,34] In particular, since the fused salphen-phenazine-NDI motif has an electric dipole moment, this provides a handle for functionalization and chemical engineering by steric control for steering the packing. The stability of this molecule is another attractive feature. Self-organization is driven by supramolecular noncovalent interactions such as π-π stacking, hydrogen bonding, and a hydrophobic packing environment. To design a supramolecule with a designated

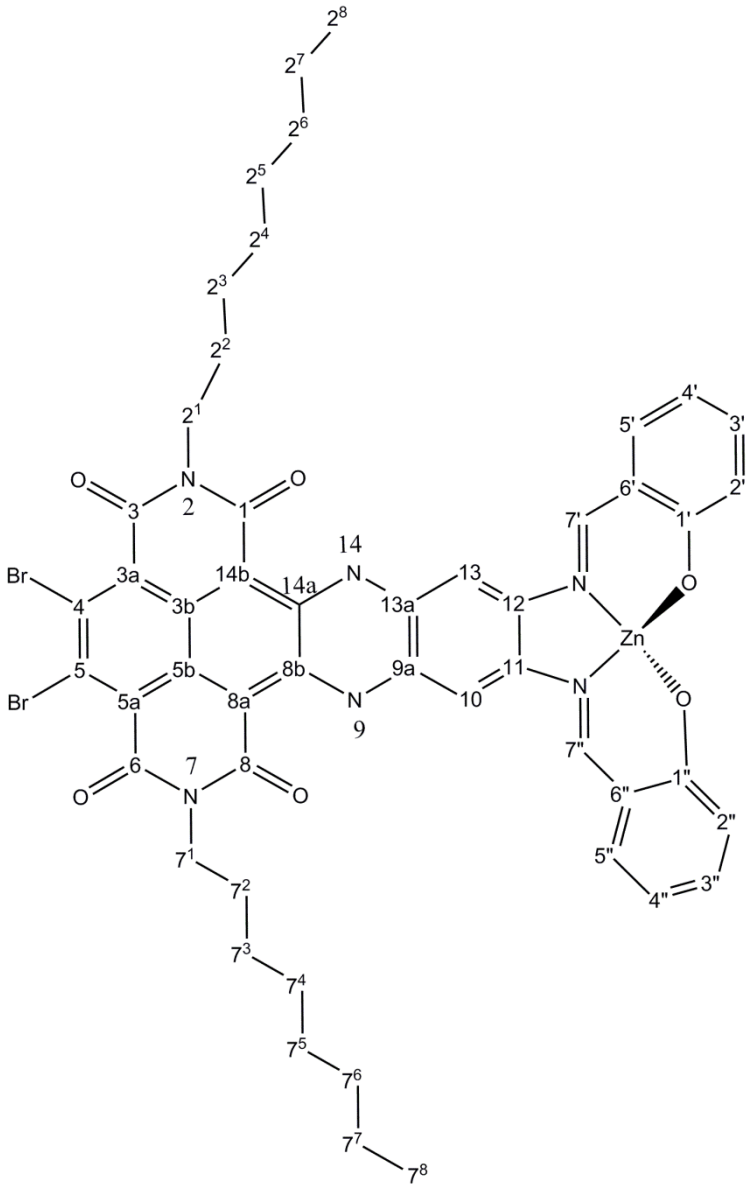

Figure 4.1 Chemical structure of the DATZnS(4H) molecule with numbering according to the IUPAC convention. DATZnS(4H) is a member of a class of fused NDI-zinc-salphen based chromophore (salphen = bis-salicylimide phenylene) which are catching interest in the field of chemical design of light harvesting antenna molecules. These molecules are both robust and versatile with respect to optical tuning and other chromophoric chemical properties. The dipole moment of the molecule is aligned along the principal axis of the molecule.

property like efficient light harvesting, we have to deepen our knowledge about how molecular characteristics influence the self-assembly.[35] The DATZnS(4H) dyad has the possibility to be tailored for incorporation into flexible large area devices. Compact π-π stacking arising from the phenazine helps to form a rigid scaffold to attach the catalyst.[36] The wavelength at which photons are absorbed in

the dyad can be adjusted with the functional groups so that it can cover the broad range of the solar spectrum. The introduction of different metals in the salphen[18] part can be used to tune the photophysical and electronic properties.[37,38] Finally, these systems can produce the high chromophore density that is considered essential for efficient light harvesting, as explained in chapter 2.

To mimic the engineering principles of nature we have to understand how the molecules can be packed.[39] Moreover, packing studies are essential for getting insight in to the solid state physical properties of aggregates. Overall dimensions and shapes of the final assemblies are determined by various packing factors, both steric and electronic. A supramolecular strategy based on DATZnS(4H) with diverse functional groups offers the opportunity to steer the packing in desired directions. In parallel, profound mechanistic insight into packing effects will pave the way for investigating and optimizing the functional properties using theoretical and experimental studies ahead of experimental realization.

Computational integration of CP/MAS NMR and Cryo-EM for resolving the packing is opening a new horizon to visualize supramolecular structures with well defined scaffolding and intrinsic heterogeneity at the molecular level.[39] By carefully analyzing regions of nonzero diffraction in reciprocal space, either obtained directly from electron diffraction or indirectly from Fourier transforms of TEM images, packing order can be detected and combined with chemical shift and distance constraints obtained by MAS NMR to average static heterogeneity and resolve a very detailed model for the supramolecular organization in the absence of true translation symmetry. In chapter 2, it is explained how the systematic absences in reciprocal space can be acquired by Cryo-EM. Along with chemical shift information and distance constraints obtained by CP/MAS NMR and ^{1}H-^{13}C heteronuclear correlation spectroscopy data collected from samples with ^{13}C at natural abundance, a space group could be identified. In chapter 3, electron nano crystallography is used to determine the unit cell parameters and space group, while the packing is filled in combination with CP/MAS NMR. In this chapter, it is shown that very limited Cryo-EM, in combination with chemical shift and HETCOR data can guide the state of the art molecular mechanics modeling of the packing organization in a periodic framework with limited correlation length. Spatial correlation peaks are obtained from HETCOR data collected at longer mixing time.

Here a unique unit cell with twofold axis can be deduced from EM since the NMR and DFT modeling point to C_2 molecular symmetry of the DATZnS(4H) and a racemic packing of the delta and lambda forms. The unit cell parameters are optimized using the FORCITE module in the Materials Studio software. In addition, the principle reflection in reciprocal space deduced from the EM was reproduced using Crystal Maker to validate the packing. Finally it is tempting to conclude that steric control by bulky substituents allows for a switch between parallel and antiparallel stacking of the DATZnS motif.

4.2 Results

4.2.1 Chemical shift assignments

DATZnS(4H) is a fused NDI-zinc-salphen based chromophore (salphen = bis-salicylimide phenylene). Moderately sized molecules like DATZnS(4H) with low symmetry and few protons, which are on the extended network of conjugated aromatic rings, make it feasible to identify selective intermolecular polarization transfer events, to spatially probe the structure.[40] ^{13}C 1D CP/MAS NMR data were collected to start with the structural analysis (Figure S4.1). The spectrum is well dispersed over 170 ppm, which makes a reasonable assignment based on chemical shifts possible. This dispersion of chemical shifts is achieved through rich functionalities, as there are four carbonyl groups, two phenoxy, and two imide groups present in the fused NDI-zinc-salphen based chromophore. The narrow lines in the 1D CP/MAS NMR spectrum point to a homogeneous, nearly crystalline microstructure.

CP/MAS NMR ^{13}C chemical shifts σ_i^C were assigned by comparison with computational chemical shifts using Gaussian 03 and solution state NMR of the DATZnSTP molecule introduced in chapter 2 (Table 4.1). Assignments of the primary, secondary and tertiary carbon atoms can be confirmed with the aid of HETCOR data acquired with a short mixing time of 0.256 ms, to limit spin diffusion through intermolecular pathways (Figure 4.2). The spectrum is divided into two panels for the aliphatic region and the aromatic region. The aliphatic region is spread from 10 ppm to 50 ppm, while the aromatic region is from 100 ppm to 170 ppm. The aromatic CH protons are reasonably resolved in the HETCOR spectra,

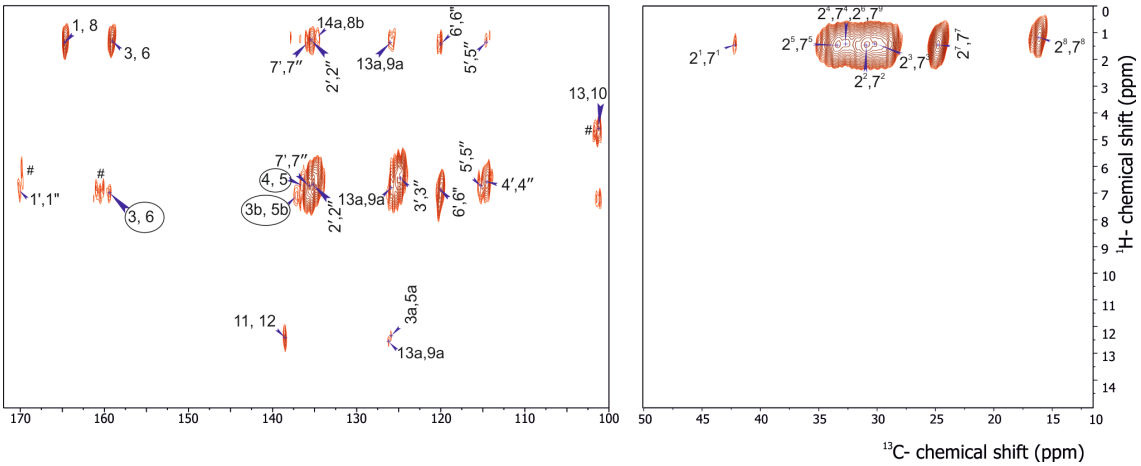

Figure 4.2 Contour plot sections of ^{1}H-^{13}C heteronuclear dipolar correlation spectra at 2 ms, which is showing long range correlations signals recorded in a field of 17.6 T by using a spinning frequency of 13 kHz. The spectrum is divided over two panels, aliphatic on the right and aromatic on the left. Folding of the tails along the phenazine can be deduced from a set of correlation peaks between the ^{1}H from the aliphatic tail and the ^{13}C on the phenazine backbone. Formation of a pseudo octahedral recognition motif involving the Zn^{2+} and the two bromine of adjacent molecules transpires from an intermolecular correlation indicated by circles arising from the interaction between salphen and NDI. # indicates the side bands.

and the data are well in line with the results from the computational chemical shift (Table 4.1). The terminal methyl group in the alkyl chain has a characteristic shift of 13.7 ppm, while the alkyl group attached to the electronegative nitrogen resonates with a chemical shift of 40.7 ppm. The 2^{7}, 7^{7} responses are well resolved with identical shifts of 22.6 ppm, revealing symmetry in the molecule and in the packing. The 13, 10 in the phenazine ring are also symmetry related and have a characteristic shift of 100.1 ppm.

4.2.2 Analysis of HETCOR at longer mixing time

In the HETCOR spectra at longer mixing time, there are many long-range correlation signals arising from the heteronuclear dipolar transfer between proton and carbon nuclei, which could be inter or intramolecular (Figure 4.2).[39] For the DATZnS(4H) molecule the protons attached to the tertiary carbon nuclei are well resolved in the 2D HETCOR at short mixing times (Figure S4.2). This is important for the selective detection of long range correlations at a cross polarization time of 2 ms, to resolve the spatial arrangement of the DATZnS(4H) molecules in the

Table 4.1 Experimental CP/MAS NMR chemical shifts compared with computational results from Gaussian 03 calculations for the DATZnS(4H).

Position	$\sigma^{C}_{DATZnS(4H),\ expt}$	$\sigma^{C}_{cDATZnS(4H),\ calc}$
1, 8	163.6	162.5
3, 6	158.3	157.8
4, 5	135.4	152.3
14b, 8a	99.0	101.7
14a,8b	133.5	136.7
3a, 5a	124.8	125.1
3b, 5b	136.1	130.7
13a, 9a	125.0	128.1
13, 10	100.3[1]	99.1
11, 12	137.5	140.4
1', 1''	169.1	176.2
2', 2''	133.9[1]	129.2
3', 3''	123.6[1]	128.4
4', 4''	113.6[1]	104.8
5', 5''	113.9[1]	120.6
6', 6''	118.9	107.8
7', 7''	134.3[1]	139.5
2^1, 7^1	46.40	42.4
2^2, 7^2	31.75	28.6
2^3, 7^3	31.86	28.1
2^4, 7^4	33.63	30.7
2^5, 7^5	30.85	31.8
2^6, 7^6	37.79	30.7

2^7, 7^7	26.31	23.2
2^8, 7^8	14.44	13.7

[1]Assignment based on the computational chemical shift and HETCOR at short mixing time of 0.256 ms.

packing.

Long-range correlations between protons attached to the carbon atoms on the tail with the 1, 8, 3, 6 carbonyl group and aliphatic tail are observed in the HETCOR dataset collected with 2 ms mixing time. These can be intramolecular. For instance, the carbonyl group could get polarization from the 2^1, 7^1 CH_2 alkyl groups over an intramolecular distance of less than 4 Å, depending on the conformation. The transfer of polarization from protons on the alkyl chain to 14a, 8b, 13a, 9a, 6′, 6′′ 5′, 5′′ 2′, 2′′, 7′ and 7′′ carbon nuclei gives information about the folding and positioning of the tails in the packing. While transfer to 14a, 8b, 13a, 9a ^{13}C could be intramolecular or intermolecular, intramolecular transfer to 6′, 6′′, 5′, 5′′, 2′, 7′ is difficult, and the correlations point to intermolecular transfer and antiparallel stacking. Heteronuclear correlation signals involving the quaternary ^{13}C in the highly unsaturated NDI part and the salphen are very useful for structure determination, since there are no protons on the NDI motif for intramolecular transfer. Extensive polarization transfer from aromatic protons on the salphen part to 4, 5, 3, 6, 3b, and 5b quaternary carbon atoms corroborate an antiparallel stacking arrangement. For a cross polarization time of 2 ms, a spatial correlation is observed between the 14-NH proton and 3a, 5a, 4 and 5 ^{13}C. A rapid buildup of signal indicates it concerns primarily intramolecular transfer.

4.2.3 Cryo-EM

Stripes observed in the cryo-EM image lead to two strong reflections in the Fourier transform that give information about the periodic arrangement (Figure 4.3). These spots correspond to a distance of 1/1.87 nm. They occur in various images, indicating periodic repetition of the molecule in a preferred orientation.(data not shown) Since no other distinct spacing could be observed in the TEM images, there is considerable heterogeneity in the sample and packing.

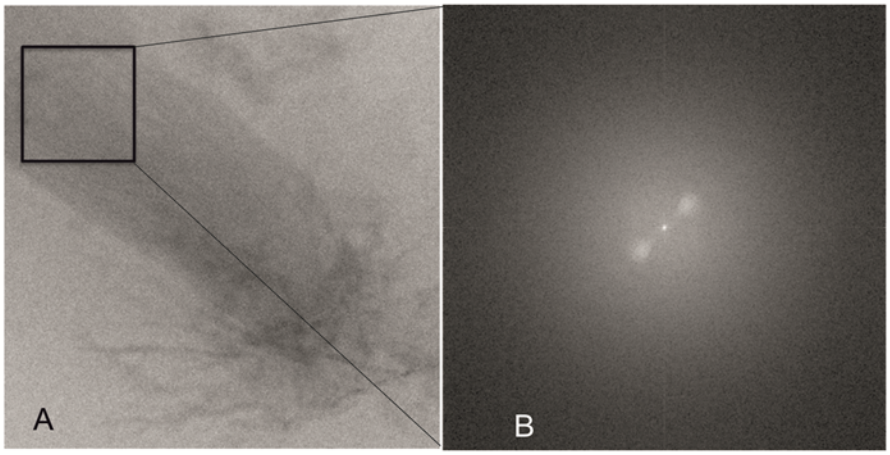

Figure 4.3 (A) TEM image of the DATZnS(4H) loaded on a carbon grid revealing a lamellar arrangement. (B) Fourier transform of the selected region indicated with a black square shows a 1.87 nm periodic repetition

4.3 Discussion

4.3.1 Structure determination of DATZnS(4H)

Since there is only one set of NMR signals for the two halves of the molecule, this reveals molecular symmetry, either nonchiral σ_v or chiral C_2, with the latter being the lowest in energy according to DFT calculations. This imposes a twofold molecular axis, while the molecules should form lamellar packing according to the TEM. To model the structure, a homology approach is employed. The molecule was placed with its C_2 symmetry axis on the twofold axis of a unit cell of the P2/c space group. The cell parameters from the DATZnS(3′-NMe) homologue were used, and the DATZnS(4H) was positioned in the cell on the twofold axis. One molecule corresponds to twice the asymmetric unit and to eliminate the spurious images, the unit cell was converted to *P*1. The redundant fragments were selected and deleted and the cell was converted back to *P*2/*c* with the find symmetry command in Materials Studio. Two settings were considered, the original setting with parallel stacking and a setting, where the *a* and *c* axis were interchanged to get antiparallel stacking (Figure S4.3). Optimizations of unit cell parameters and molecule were performed with FORCITE in Materials Studio for both settings and it was found that the antiparallel stacking is stabilized by 37 kcal/mol with parameters a = 1.47 nm, b = 1.83 nm, c = 9.6 nm, α = 90°, β = 109° and γ = 90° (Figure 4.4).

The antiparallel model in Figure 4.4 contrasts with the parallel stacking deduced for the DATZnS(3′-NMe) homologue in chapter two, where only correlations were observed between the NDI motif and the dimethylamine functionalities, which are thought to play a decisive role in steering the packing configuration of the latter compound. The extensive polarization transfer to 4, 5, 3, 6, 3b, and 5b from aromatic protons on the salphen part to the NDI part indicated in Figure 4.2 with a circle confirms the antiparallel stacking, which has short distances of ~3.5-4 Å between the salphen protons and NDI carbons. This matches very well with the heteronuclear distance determined from the quantitative numerical analysis of LGCP buildup curves in the related DATZnS(3′-NMe) compound in Figure 2.3 in chapter 2. The alternative, recognition between the NDI and the salphen part with extended overlap in the parallel stack model is difficult to reconcile with the characteristic heteronuclear transfer in Figure 4.2, since in the parallel model for the DATZnS(4H) not only the enthalpy is higher in the modeling because of steric hindrance but also the distances are larger, in the range of 5 Å. Finally, the HETCOR data for the DATZnS(3′-NMe) homologue in chapter 2 do not exhibit the characteristic correlations indicated with the circle in Figure 4.2 Thus, the heteronuclear transfer from the salphen to the NDI is a critical observation for structure validation.

4.3.2 Insight into packing

The structure shows π-π overlap between the phenazine moieties, which may help to drive the packing along the *b* axis. The distance between two molecules in the direction perpendicular to the plane of the molecule is 0.36 nm,[41] indicating strong π - π stacking. The tails are projecting outwards into the space between the two stacks. The ring structure locks the keto group into co-planarity with the phenazine ring resulting in substantial π-electron conjugation involving the keto and the phenazine ring. The presence of the carbonyl group and the nitrogen with the lone pair induces an extended π electron delocalization. Due to this extended conjugation phenazine derivatives adopt a planar geometry.[42,43] The electropositive Zn^{2+} in the Λ and Δ chiral salphen functionalities produce a cavity to which the electronegative bromine of the next molecule along the *c* axis is attracted to form the pseudo-octahedral recognition motif, similar to the

DATZnS(3′-NMe) homologue (Chapter 2). This electrostatic attraction and head to tail alignment of electric diploes can help to stabilize the packing along the axial direction of the molecule. The pseudo octahedral coordination of the zinc follows

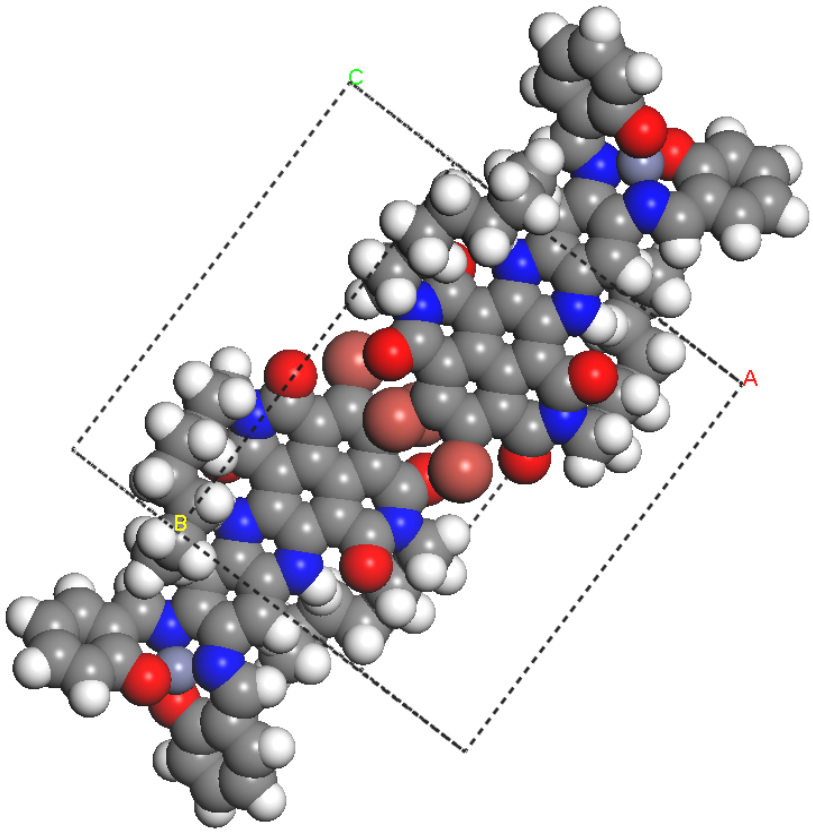

Figure 4.4 Proposed structure of antiparallel DATZnS(4H) in a 3D packing with the space group *P*2/c. In comparison with the parent structure of the DATZnS(3′-NMe) homologue in chapter 2, the dipole moments are compensated between the stacks and antiparallel rows of head to tail DATZnS(4H). Since the only difference between the two compounds is the NCH_3 functional groups, chemical control over the dielectric characteristics at the supramolecular level is achieved.

the packing induced chirality with enantiomeric pairs of lambda and delta form alternating along the antiparallel stack.

In the TEM pattern of Figure 4.3, the stripes are from alternating regions of high electron density containing Zn^{2+} with regions of phenazine. Along the antiparallel stack the dipole moments are aligned in the opposite directions, which constitute the scaffold of the packing. With the dipoles compensated at the level of the antiparallel arrangement within the stack, there is no emerging electrostatic component for stabilization of planes as in the DATZnS(3′-NMe) homologue. This

may explain why the DATZnS(4H) structure appears much less ordered in the TEM, with only the two reflections of the long repeat along the *c* axis in the Fourier transform. Tight packing of dyads within the self-assembled stacks provides a high chromophore density to harvest the solar light efficiently. The pseudo-octahedral recognition motif is a characteristic of the supramolecular packing, and is consistent with the antiparallel arrangement that transpires from the spatial correlation peaks between salphen and NDI. The structure accommodates the folding of the tails along the phenazine, in line with the HETCOR data at longer mixing time. Steric hindrance from the salphen part restricts parallel stacking.

4.4 Conclusions

Based on the energy, density, intermolecular correlations from CP/MAS, reflection spots in the Fourier transform of the TEM image and homology modelling, we converge upon an antiparallel stacking for the DATZnS(4H) forming lamellar sheets in a $P2/c$ packing arrangement. Pseudo-octahedral coordination of the Zn^{2+} and C_2 molecular symmetry produces the twofold axis, while the two enantiomeric forms Λ and Δ produced by a *c*-glide symmetry operation lead to a racemic packing with the alkyl chains folded along the phenazine. This structure is a homologue of the DATZnS(3′-NMe) structure determined in chapter 2, and suggests that the NCH_3 functional group can be used to steer the aggregation from a parallel sheet in DATZnS(3′-NMe) to an antiparallel sheet in DATZnS(4H). This concept paves the way for the chemical design of supramolecular scaffolds for light harvesting and charge separation, on the way to organic solar fuel cell device concepts that can be programmed to quench the internal field in an antiparallel arrangement, *e.g.* for light harvesting, or exploit the internal field from aligned dipole moments, *e.g.* for the injection of charge in catalysts for water splitting. With access to detailed structure information of heterogeneous supramolecular assembly in the DATZnS(4H), rational design of functional based material for light harvesting and charge separators may become reality.

4.5 Materials and methods

4.5.1 Sample preparation

8,9-Dibromo-5,12-dihydro-5,12-diazatetracene di-*n*-octylimide diamine intermediate (103 mg, 0.13 mmol), prepared from 2,3-(*p*-Toluenesulfonamido)-8,9-dibromo-5,12-dihydro-5,12-diazatetracene di-*n*-octylimide was dissolved in 9 mL dry, degassed DMF under an Ar atmosphere and heated to 80 °C in the dark.[44] In a separate flask, salicylaldehyde (40 mg, 0.33 mmol) and zinc acetate dihydrate (265 mg, 1.32 mmol) were dissolved in dry, degassed DMF (5 mL) and kept under Ar. This mixture was stirred for 5 minutes and added to the hot DMF solution via a syringe. After 6 hours, the reaction mixture was cooled down to room temperature, diluted with 5 mL H_2O and stored overnight at -20 °C to induce precipitation. The dark blue precipitate was collected on a filter and washed with water, ethanol and dichloromethane to afford (after vacuum drying) 89 mg of a dark blue solid (59 % yield from 8,9-Dibromo-5,12-dihydro-5,12-diazatetracene di-*n*-octylimide-diamine). IR (ATR FTIR): 2953, 2922, 2851, 1686, 1572, 1528, 1499, 1448, 1431, 1315, 1281, 1225, 1200, 1173, 1150, 1128, 1105, 1076, 1030, 964, 914, 847, 584 cm^{-1}. Mp > 300 ° C

4.5.2 NMR measurements

The solid-state CP/MAS spectra were recorded with a 750 MHz spectrometer, equipped with 4 mm triple resonance CP/MAS probes in dual ^{1}H-^{13}C mode with a spinning frequency of 13 kHz ± 5 Hz. The pulse sequence for the 2-D heteronuclear polarization transfer experiment is shown in Figure S4.3. The 2D sequence starts with a magic angle preparation pulse on the ^{1}H channel, followed by FSLG LGCP to transfer the magnetization from the protons to carbons during a variable time t_1. The ^{1}H dimension of the heteronuclear dipolar interaction correlation experiment can be obtained by Fourier transformation with respect to t_1. The TPPM scheme was used to decouple proton spins during acquisition while the ^{13}C free induction decays (FIDs) were recorded in the t_2 domain (Figure S4.4). For short range polarization transfer from ^{1}H directly bonded to ^{13}C, a CP contact time of 0.256 ms was used, and for longer range polarization transfer and the detection of intermolecular correlations, a CP time of 2 ms was employed. The ^{1}H chemical shift

was calibrated from a spectrum of solid tyrosine-HCl salt.[40] A scale factor of 0.57 for the FSLG was verified with solid tyrosine HCl salt. The data were processed using the Bruker TopSpin 3.2 software (Bruker, Billerica, MA).

4.5.3 Cryo-EM measurements

For electron microscopy, samples dissolved in ethanol were applied to a carbon grid at 83 K with a Vitrobot vitrification system (FEI, Hillsboro, OR). Electron microscopy was done with a Tecnai G2 Polara electron microscope (FEI, Hillsboro, OR) equipped with a Gatan energy filter at 115,000 magnification (Gatan, Pleasanton, CA). Images were recorded in the zero-loss imaging mode, by using a slit width of 20 eV, with a slow-scan CCD camera at 1 micrometer under focus, to have optimal phase contrast transfer at 300 kV.

4.5.4 Structure modeling and chemical shift calculation

Computational chemical shifts were obtained with the Gaussian 03 software package (Gaussian, Inc., Wallingford, CT) using the Becke, Lee, Yang, and Parr (BLYP) exchange-correlation functional with 6-311G basis set. The molecule was geometrically optimized prior to NMR chemical shift calculation.

Biovia Materials Studio Suite (Biovia, San Diego, CA) was used for computational modeling. A monomer structure of the DATZnS(4H) core without the aliphatic tails was obtained by optimization with Gaussian 03 (Gaussian, Inc., Wallingford, CT) and placed in the *P*2/c unit cell determined for the homologue in chapter 2 as described in the results section. Optimization of the cell parameters was performed with the FORCITE module. For geometry optimization with Forcite, the "smart" algorithm setting in materials studio was used and a convergence tolerance of 0.001 kcal/mol for energy and 0.5 kcal/mol/Å for the force parameter were applied. For the full molecule including the tails, DMol^3 calculations were conducted to get the ESP charges. The generalized gradient approximation (GGA) with the Perdew Burke Ernzerhof (PBE) functional with double numerical atomic orbital augmented by a polarization p-function (DNP) basis set was used for DMol^3 calculations.

References

(1) Purchase, R. L.; de Groot, H. J. M. *Interface Focus* **2015**, *5*.

(2) Listorti, A.; Durrant, J.; Barber, J. *Nat Mater* **2009**, *8*, 929.

(3) House, R. L.; Iha, N. Y. M.; Coppo, R. L.; Alibabaei, L.; Sherman, B. D.; Kang, P.; Brennaman, M. K.; Hoertz, P. G.; Meyer, T. J. *Journal of Photochemistry and Photobiology C: Photochemistry Reviews* **2015**, *25*, 32.

(4) Wigginton, N. S. *Science* **2016**, *352*, 1185.

(5) Wong, K.-T.; Bassani, D. M. *NPG Asia Mater* **2014**, *6*, e116.

(6) Yoneda, Y.; Noji, T.; Katayama, T.; Mizutani, N.; Komori, D.; Nango, M.; Miyasaka, H.; Itoh, S.; Nagasawa, Y.; Dewa, T. *Journal of the American Chemical Society* **2015**, *137*, 13121.

(7) Blankenship, R. E.; Olson, J. M.; Miller, M. In *Anoxygenic Photosynthetic Bacteria*; Blankenship, R. E., Madigan, M. T., Bauer, C. E., Eds.; Springer Netherlands: Dordrecht, 1995, p 399.

(8) Hermant, R. M.; Liddell, P. A.; Lin, S.; Alden, R. G.; Kang, H. K.; Moore, A. L.; Moore, T. A.; Gust, D. *Journal of the American Chemical Society* **1993**, *115*, 2080.

(9) van Gammeren, A. J.; Hulsbergen, F. B.; Erkelens, C.; de Groot, H. J. M. *JBIC Journal of Biological Inorganic Chemistry* **2004**, *9*, 109.

(10) Gust, D.; Moore, T. A.; Moore, A. L. *Accounts of Chemical Research* **2001**, *34*, 40.

(11) Stanier, R. Y.; Smith, J. H. C. *Biochimica et Biophysica Acta* **1960**, *41*, 478.

(12) Pandit, A.; de Groot, H. J. M. *Photosynthesis Research* **2012**, *111*, 219.

(13) McConnell, I.; Li, G.; Brudvig, G. W. *Chemistry & biology* **2010**, *17*, 434.

(14) Schmid, S. A.; Abbel, R.; Schenning, A. P. H. J.; Meijer, E. W.; Herz, L. M. *Energy transfer processes along a supramolecular chain of π-conjugated molecules*, 2012; Vol. 370.

(15) Blankenship, R. E. *Proceedings of the National Academy of Sciences* **2015**, *112*, 13751.

(16) Zuber, H. *Trends in Biochemical Sciences* **1986**, *11*, 414.

(17) Barber, J.; Tran, P. D. *Journal of the Royal Society Interface* **2013**, *10*, 20120984.

(18) Hui, J. K. H.; Yu, Z.; MacLachlan, M. J. *Angewandte Chemie International Edition* **2007**, *46*, 7980.

(19) Taherimehr, M.; Decortes, A.; Al-Amsyar, S. M.; Lueangchaichaweng, W.; Whiteoak, C. J.; Escudero-Adan, E. C.; Kleij, A. W.; Pescarmona, P. P. *Catalysis Science & Technology* **2012**, *2*, 2231.

(20) Bhattacharjee, C. R.; Chakraborty, S.; Das, G.; Mondal, P. *Liquid Crystals* **2012**, *39*, 1435.

(21) Sakakibara, K.; Hill, J. P.; Ariga, K. *Small* **2011**, *7*, 1288.

(22) Etheridge, F. S.; Fernando, R.; Golen, J. A.; Rheingold, A. L.; Sauve, G. *RSC Advances* **2015**, *5*, 46534.

(23) Scholes, G. D.; Fleming, G. R.; Olaya-Castro, A.; van Grondelle, R. *Nat Chem* **2011**, *3*, 763.

(24) Paudel, K.; Johnson, B.; Thieme, M.; Haley, M. M.; Payne, M. M.; Anthony, J. E.; Ostroverkhova, O. *Applied Physics Letters* **2014**, *105*, 043301.

(25) Whiteoak, C. J.; Salassa, G.; Kleij, A. W. *Chemical Society Reviews* **2012**, *41*, 622.

(26) Şener, M.; Strümpfer, J.; Timney, J. A.; Freiberg, A.; Hunter, C. N.; Schulten, K. *Biophysical Journal* **2010**, *99*, 67.

(27) Haferkamp, S.; Haase, W.; Pascal, A. A.; van Amerongen, H.; Kirchhoff, H. *The Journal of Biological Chemistry* **2010**, *285*, 17020.

(28) Unver, E. K.; Tarkuc, S.; Udum, Y. A.; Tanyeli, C.; Toppare, L. *Journal of Polymer Science Part A: Polymer Chemistry* **2010**, *48*, 1714.

(29) Hoffmann, M.; Wilson, C. J.; Odell, B.; Anderson, H. L. *Angewandte Chemie International Edition* **2007**, *46*, 3122.

(30) Uetomo, A.; Kozaki, M.; Suzuki, S.; Yamanaka, K.-i.; Ito, O.; Okada, K. *Journal of the American Chemical Society* **2011**, *133*, 13276.

(31) Wang, C.-L.; Hu, J.-Y.; Wu, C.-H.; Kuo, H.-H.; Chang, Y.-C.; Lan, Z.-J.; Wu, H.-P.; Wei-Guang Diau, E.; Lin, C.-Y. *Energy & Environmental Science* **2014**, *7*, 1392.

(32) Son, H.-J.; Jin, S.; Patwardhan, S.; Wezenberg, S. J.; Jeong, N. C.; So, M.; Wilmer, C. E.; Sarjeant, A. A.; Schatz, G. C.; Snurr, R. Q.; Farha, O. K.; Wiederrecht, G. P.; Hupp, J. T. *Journal of the American Chemical Society* **2013**, *135*, 862.

(33) Lambert, N.; Chen, Y.-N.; Cheng, Y.-C.; Li, C.-M.; Chen, G.-Y.; Nori, F. *Nat Phys* **2013**, *9*, 10.

(34) Zhang, L.; Silva, D.-A.; Zhang, H.; Yue, A.; Yan, Y.; Huang, X. *Nat Commun* **2014**, *5*.

(35) Traub, M. C.; DuBay, K. H.; Ingle, S. E.; Zhu, X.; Plunkett, K. N.; Reichman, D. R.; Vanden Bout, D. A. *The Journal of Physical Chemistry Letters* **2013**, *4*, 2520.

(36) Kato, M.; Kosuge, C.; Yano, S.; Kimura, M. *Acta Crystallographica Section C %@ 0108-2701* **1998**, *54*, 621.

(37) Vagin, S. I.; Reichardt, R.; Klaus, S.; Rieger, B. *Journal of the American Chemical Society* **2010**, *132*, 14367.

(38) Salassa, G.; Coenen, M. J. J.; Wezenberg, S. J.; Hendriksen, B. L. M.; Speller, S.; Elemans, J. A. A. W.; Kleij, A. W. *Journal of the American Chemical Society* **2012**, *134*, 7186.

(39) Ganapathy, S.; Sengupta, S.; Wawrzyniak, P. K.; Huber, V.; Buda, F.; Baumeister, U.; Würthner, F.; de Groot, H. J. M. *Proceedings of the National Academy of Sciences* **2009**, *106*, 11472.

(40) Van Rossum, B. J.; Förster, H.; De Groot, H. J. M. *Journal of Magnetic Resonance* **1997**, *124*, 516.

(41) Polander, L. E.; Pandey, L.; Romanov, A.; Fonari, A.; Barlow, S.; Seifried, B. M.; Timofeeva, T. V.; Brédas, J.-L.; Marder, S. R. *The Journal of Organic Chemistry* **2012**, *77*, 5544.

(42) Schafer, B.; Gorls, H.; Presselt, M.; Schmitt, M.; Popp, J.; Henry, W.; Vos, J. G.; Rau, S. *Dalton Transactions* **2006**, 2225.

(43) Wozniak, K.; Kariuki, B.; Jones, W. *Acta Crystallographica Section C* **1991**, *47*, 1113.

(44) Rombouts, J. A.; Ravensbergen, J.; Frese, R. N.; Kennis, J. T. M.; Ehlers, A. W.; Slootweg, J. C.; Ruijter, E.; Lammertsma, K.; Orru, R. V. A. *Chemistry – A European Journal* **2014**, *20*, 10285.

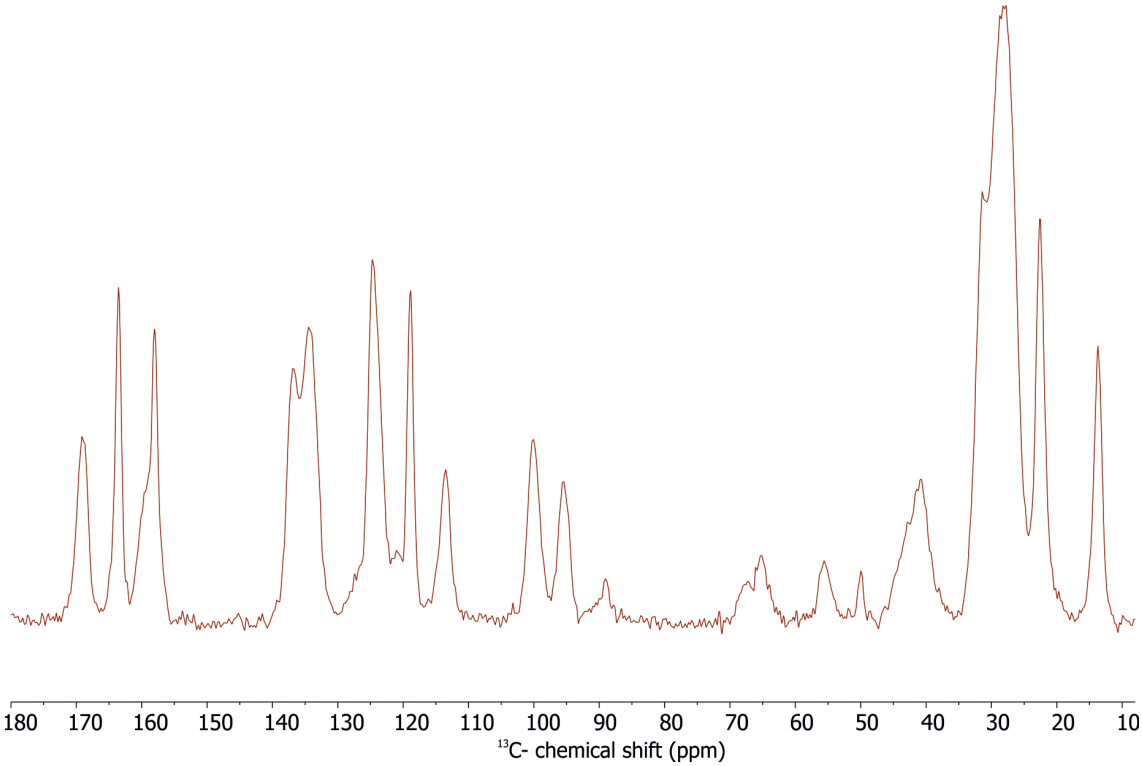

Figure S4.1 1D ^{13}C CP/MAS spectrum of DATZnS(4H) recorded at 750 MHz.

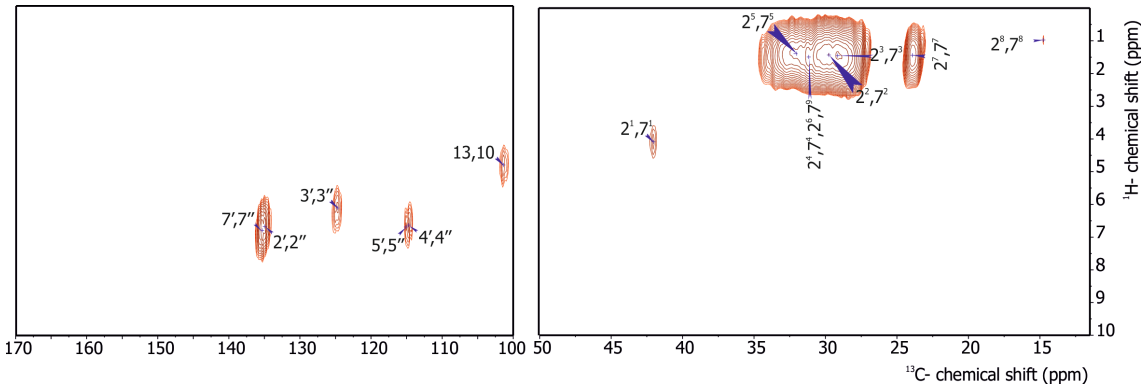

Figure S4.2 HETCOR spectra of the DATZnS(4H) at a short mixing time of 0.256 ms.

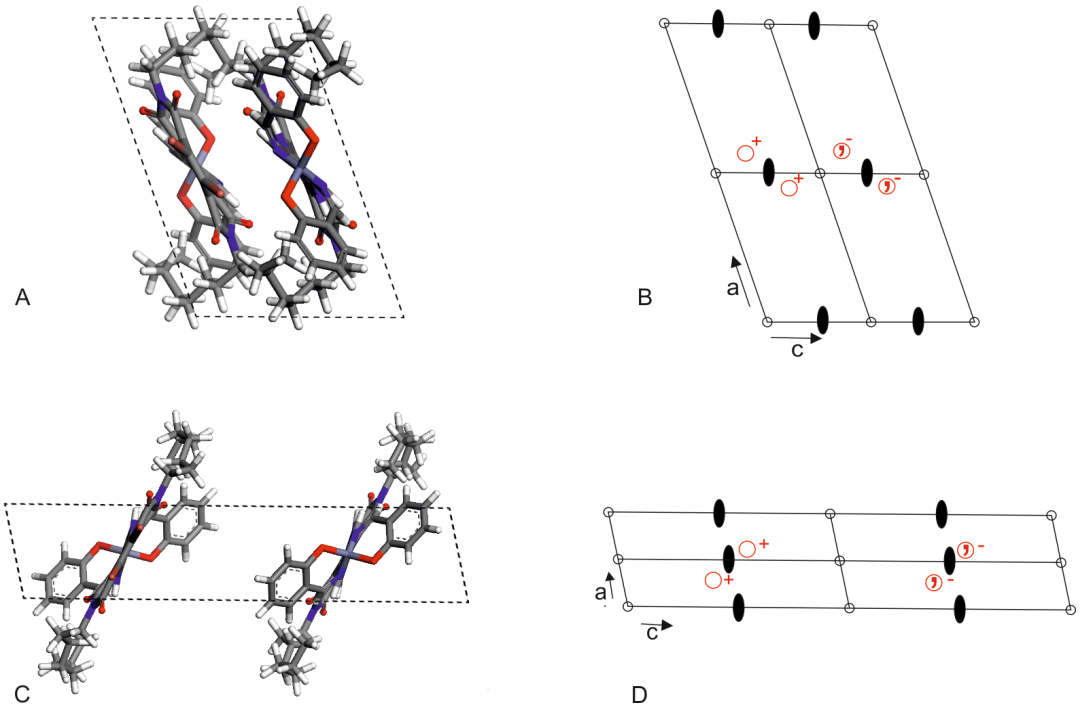

Figure S4.3 ● indicates the two fold axis, ○ indicates the inversion point, ○+ and ◑- indicates enantiomers running in mutually opposite direction. The parallel stacking (A) an antiparallel stacking (C) molecules in the unit cell observed along the 'b' axis with their respective space group diagram (B and D).

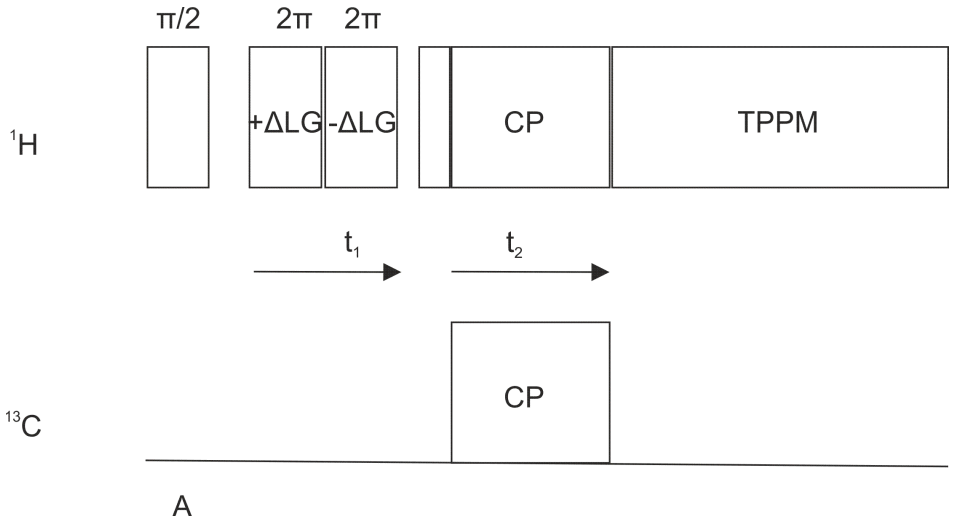

Figure S4.4 Pulse sequence used for the HETCOR experiment.